IEEE Access
Multidisciplinary ⋮ Rapid Review ⋮ Open Access Journal

Received 14 October 2024, accepted 8 December 2024, date of publication 11 December 2024, date of current version 20 December 2024.

Digital Object Identifier 10.1109/ACCESS.2024.3515644

RESEARCH ARTICLE

Advancing Medical Catheter Navigation: Design, Optimization, and Control of a Magnetic Tractor Beam (MTB) Handheld Device

CHAYABHAN LIMPABANDHU AND ZION TSZ HO TSE

Centre for Bioengineering, School of Engineering and Materials Science, Queen Mary University of London, E1 4NS London, U.K.

Corresponding author: Zion Tsz Ho Tse (z.tse@qmul.ac.uk)

This work was supported in part by the Academy of Medical Sciences Professorship, Royal Society Wolfson Fellowship; in part by the Cancer Research U.K., National Institutes of Health (NIH) Bench-to-Bedside Award under Grant EDDPMA-Nov21\100026; in part by the NIH Center for Interventional Oncology under Grant ZID# BC011242 and Grant CL040015; and in part by the Intramural Research Program of the National Institutes of Health.

ABSTRACT The progress of medical procedures towards minimally invasive techniques has led to notable advancements in medical device engineering, particularly in the navigation and control of catheters within complex anatomical structures. This study introduces a novel handheld device using the Magnetic Tractor Beam (MTB) that aims to improve the accuracy and safety of catheter navigation during lung interventions. The device aims to overcome the limitations of traditional catheterisation, which include restricted manoeuvrability and the potential for tissue damage, by utilising magnetic fields to manipulate catheters without direct contact. The device focuses on user-centric design and uses iterative feedback to improve its functionality. The device's efficacy in achieving precise control over catheter movement is demonstrated through comprehensive experiments, with a particular focus on navigating the complex pathways of the respiratory system. The experimental setup comprises the fabrication of a trachea and bronchi model using 3D printing, the refinement of magnetic configurations to achieve the highest possible MTB effect, and thorough testing to verify the precision and control mechanisms of the device. The results demonstrate a notable enhancement in the rates of successful navigation and a decrease in the possibility of tissue perforation. The study highlights the significance of real-time imaging and accurate control in improving the effectiveness of catheter-based interventions.

INDEX TERMS Magnetic actuation catheter, magnetic catheter navigation, magnetic navigation system, medical device design, minimally invasive surgery.

I. INTRODUCTION

In lung cancer diagnosis and treatment, navigating the complex anatomy of the respiratory system presents significant challenges that impact patient outcomes and procedural safety. Traditional interventions often struggle with the precise placement of catheters due to the rigidity and limited manoeuvrability of conventional systems, leading to increased risks of tissue damage and prolonged recovery times. These procedures require a high degree of control and precision, as inaccurate catheter navigation can lead to complications such as perforation or inaccurate targeting of the treatment area. Nevertheless, the development of minimally invasive techniques [1], [2], [3], [4], [5], [6], [7], [8], [9], such as those facilitated by magnetic navigation systems [10], [11], [12], [13], has transformed patient care by minimising surgical incisions and improving recovery, underscoring the need for ongoing innovation in medical device engineering [13], [14], [15], [16], [17]. This emphasises the critical focus on enhancing accuracy and flexibility, mainly through integrating magnetic technologies that offer new possibilities for precise and safe medical interventions.

Recent advancements in magnetic navigation systems using permanent magnets have demonstrated significant

The associate editor coordinating the review of this manuscript and approving it for publication was Giambattista Gruosso.

progress in various medical applications. Systems such as the Niobe®Magnetic Navigation System have shown accurate and reproducible target navigation, enhancing the success rates of cardiac interventions [18], [19]. Additionally, magnetic propulsion systems using permanent magnets have been developed for micro-robots in human blood vessels, showcasing the potential for minimally invasive procedures with reduced risk of tissue damage [20], [21]. Furthermore, research in magnetically steerable guidewires for minimally invasive surgery has highlighted the ability to perform intricate manoeuvres in vascular and other confined spaces [22].

The MTB effect is based on using magnetic technology in medical devices [23]. This technology uses controlled magnetic fields to address the limitations of traditional catheterisation, which often relies on stiff wires and may have restricted manoeuvrability. The innovative handheld device at the core of this research embodies an interdisciplinary combination of biomedical engineering, material science, and electronics. The equipment builds upon the progress made over decades, starting with the research in magnetic resonance imaging and the refined engineering currently available in surgical robots. The device is designed using SolidWorks, incorporating the usability principles and user-centric design characteristics of modern medical device development.

The MTB technology offers several distinct advantages compared to existing catheter navigation systems. Traditional systems often depend on mechanical guidance using stiff wires, which can limit manoeuvrability and increase the risk of tissue damage. In contrast, the MTB handheld device utilises magnetic fields to manipulate catheters without direct contact at the catheter tip, allowing for smoother and more precise navigation through complex anatomical pathways. This is particularly beneficial for lung interventions, where navigating the intricate respiratory system is challenging. The MTB device is also designed to be compact, portable, and user-friendly, making it a more versatile and cost-effective solution than many current catheter navigation technologies.

Due to its control and electronic integration, the device functions as a conduit for magnetic manipulation and an interface between human intent and robotic precision. The interaction between user input and machine output is an elaborate procedure refined through numerous iterations and feedback cycles based on human-centred design principles and iterative development. The research findings provide the foundation for a medical instrument representing a significant technological advancement for bronchoscopy procedures, marked by increased safety and improved accuracy. By minimising the risk of harm and enhancing precision in medical procedures, the device embodies an advancement in patient-centred healthcare. Its compactness and portability offer significant benefits, particularly in settings where limited space and the need for mobility are crucial. These developments result from a combination of engineering innovation and clinical necessity, leading to significant improvements that enhance healthcare professionals' abilities and raise the standard of patient care.

The potential clinical implications of the MTB handheld device are substantial, especially in improving the precision and safety of lung interventions. By utilising magnetic fields to manipulate catheters without direct contact, the device reduces the risk of tissue damage and improves navigation through complex respiratory pathways. This technology can enhance patient outcomes by increasing the accuracy of catheter placement and reducing procedure times. Preliminary trials are planned to assess the device's performance in clinical settings, focusing on its efficacy in real-world medical procedures, gathering data on patient outcomes, and obtaining feedback from medical professionals. The results of these trials will provide valuable insights into the practical applications of MTB technology and guide further refinement and adoption in clinical practice.

II. METHOD AND PROCEDURES

A. MAGNETIC TRACTOR BEAM (MTB) RANGE EXPERIMENT

The MTB system is constructed using a strategic arrangement of one lead magnet and two co-lead magnets to generate the MTB effect. This configuration enables guidance and control of the catheter tip. The lead magnet, positioned at the forefront, interacts with the co-lead magnets to create a controlled magnetic field. This field exerts a magnetic force on a follower magnet embedded within the catheter, allowing for accurate manipulation and steering. The decision to use a 50mm lead diameter and a 15mm co-lead diameter, both with a thickness of 20mm, was based on selecting the best combinations. This choice was made to maximise the strength of the magnetic field and create the most significant possible distance between the lead and follower magnets. This configuration is crucial for the experiment's success and ensures a strong Magnetic Tractor Beam (MTB) effect. It optimises the magnetic force and creates conditions that facilitate achieving.

The follower magnet's diameter ranges from 6mm to 1mm to navigate the lung's complex bronchi. Minimising its size ensures versatility in different anatomical scenarios, especially when the bronchial pathways are narrow. Additionally, the follower magnet maintains a thickness of 18mm, which has been carefully determined through extensive experimentation. This thickness has been shown to induce the most stable and effective MTB effect phenomenon, enhancing the precision and reliability of the experimental setup.

The comprehensive study of these specifications highlights the complexity of optimising the device for effectiveness and versatility. The selection process was accompanied by rigorous experimentation to ensure that the chosen parameters enhance the robustness of the MTB effect and enable manoeuvrability in challenging anatomical conditions. These attempts create an extensive reference table, a valuable user tool, obtained through methodical experimentation. This guide provides a detailed explanation of the complex

relationship between the distance of the co-leads and the resulting distance between the lead and follower magnets, which is measured from one edge to the other. These insights provide users with the necessary knowledge to make informed decisions, improving the effectiveness and usefulness of the magnetic catheter system in different experimental configurations.

B. HANDHELD DEVICE

1) MODEL DESIGN

During the development of the MTB handheld device, SolidWorks was chosen as the primary design tool due to its capabilities in precise modelling and simulation. This software facilitated the integration of usability principles and user-centric design characteristics, ensuring that the device would be effective and easy to use in clinical settings. The device's design features a servo motor responsible for controlling the gripper legs, which adjusts the distance between the co-lead magnets. This setup allows for dynamic modification of the co-lead proximity, providing flexibility for various experimental configurations. The integration of SolidWorks enabled the design team to create a cohesive system where each component works together, enhancing the device's overall functionality.

Moreover, the design included the integration of a stepper motor into a 50mm linear rail to control the linear movement of the inverter magnet attached to the holder. This configuration ensures precise and stable motion, crucial for navigating complex anatomical pathways like those in the respiratory system. The linear rail is tightly attached to the holder, and the inverter magnet is securely fixed. Using motorised control for the stepper motor guarantees accurate motion of the inverter magnet along a straight path, significantly improving the overall adaptability of the device. The device achieves high adaptability and precision by using motorised control for both the servo and stepper motors, making it capable of performing intricate manoeuvres required during lung interventions. These design choices, facilitated by SolidWorks, resulted in a robust, versatile, and user-friendly device that significantly enhances catheter navigation.

2) DISTANCE BETWEEN CO-LEAD MAGNETS

The distance between co-lead magnets is calculated using measurements obtained from SolidWorks Assembly. The measurements are recorded with particular regard to detail and serve as a crucial reference, establishing a direct relationship between the servo motor's position and the distance between the co-lead magnets. The calculated distance becomes the central focus by strategically setting the initial position of the servo motor at 0° (Figure 2). It is prominently displayed on the LCD screen during operational phases. Including this real-time feedback mechanism on the LCD is crucial, providing users with a real-time and continuous perception of the exact distance between the co-lead magnets throughout the device's usage.

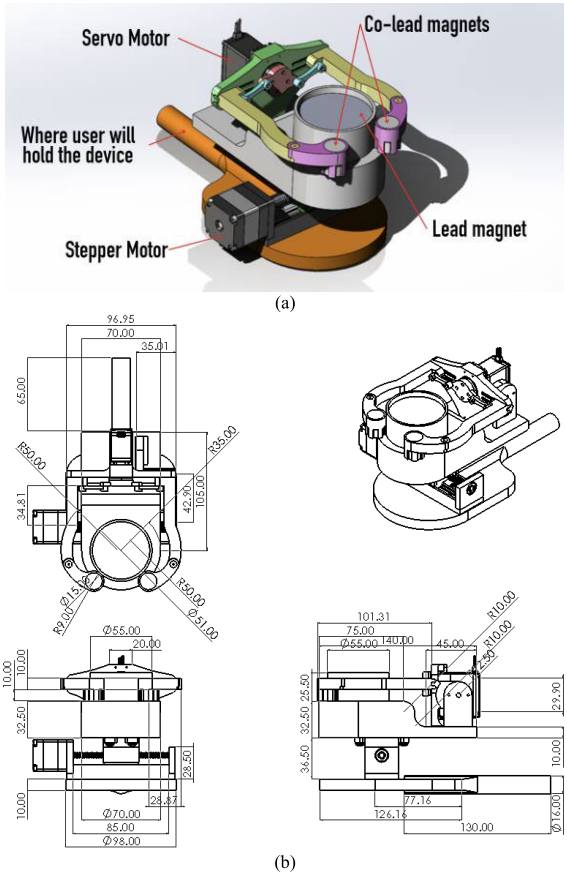

FIGURE 1. Handheld device design a) SolidWorks assembly of the device b) 2D Drawing of the device.

3) DEVICE FABRICATION

The fabrication of the device involves utilising the capabilities of both Formlabs and Ultimaker 3D printing technologies, ensuring a thorough and adaptable manufacturing process. Formlabs, known for its exceptional accuracy and detailed prints, uses resin as the primary material for printing specific parts of the device. This decision is strategic, considering the complex intricacies and precise features needed in specific design components. Ultimaker, a dependable 3D printing platform, contributes to manufacturing using Polylactic Acid (PLA) as the printing material. PLA is known for its durability and versatility, making it an exceptional option for components that necessitate sturdiness and structural integrity. The simultaneous utilisation of these two 3D printing technologies enables a collaborative strategy, leveraging the distinct advantages of each method to create a comprehensive and optimised device.

Because magnets are essential parts of the device, particular attention is paid to selecting materials to prevent any interference with their magnetic properties. Avoiding materials susceptible to magnetic attraction ensures the device's proper functioning and prevents unintended interactions. This strict approach to selecting materials aligns with the exacting standards for designing and manufacturing the

device, highlighting a dedication to excellence and optimal functionality.

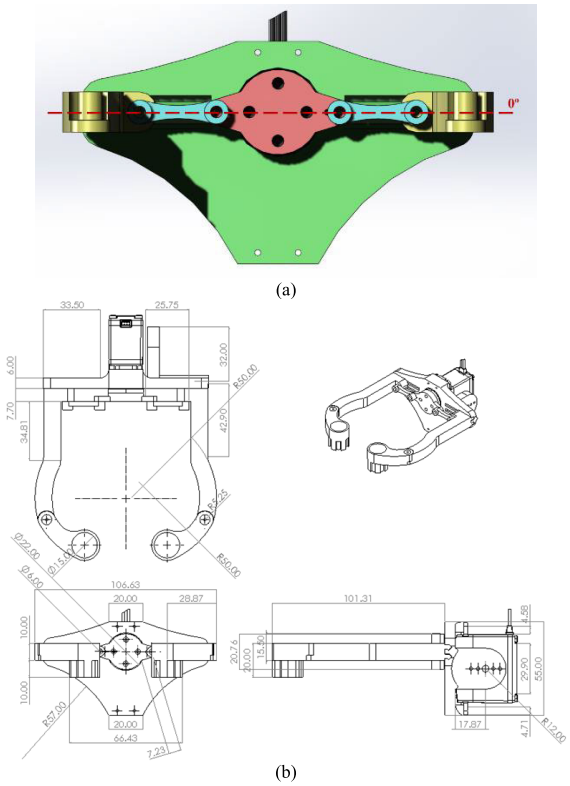

FIGURE 2. Device's gripper at its initial position a) Initial position of the servo motor at 0 degrees where the distance between co-lead magnets is at its maximum b) 2D drawing of the gripper.

4) CONTROL AND ELECTRONICS INTEGRATION FOR THE DEVICE

The design features four buttons and an LCD to enhance user interaction and operational control. The servo motor can be easily controlled using the buttons, allowing for convenient adjustment of the gripper and co-lead magnets. These buttons control the linear motion of the stepper motor, providing a user-friendly experience. In addition, the LCD functions as a dynamic interface, offering real-time feedback by displaying the distance between the co-lead magnets. This visual representation enhances user involvement and provides valuable information during experimental processes, resulting in a comprehensive and user-focused design.

The Arduino UNO R3 is connected to the servo and stepper motors through the Arduino motor shield. Simultaneously, the four buttons and the LCD are intricately connected to a specialised PCB created using Altium Designer software. The custom PCB is directly linked to the Arduino motor shield. The Arduino UNO is the central control unit for all electronic components in this design. The Arduino Integrated Development Environment (IDE) manages and coordinates the servo motor, stepper motor, four buttons, and LCD functionality. The implemented code allows users to control the movement of the two motors by pressing the assigned buttons while receiving immediate feedback on the LCD screen. This comprehensive electronic design offers an easy interface for users to navigate and guarantees accurate management of the system's components.

C. ACCURACY EXPERIMENT

An accuracy test has been performed on the device, focusing on the distance between the co-lead magnets. The distance between the co-lead magnets was adjusted randomly ten times using the handheld device at different intervals. Afterwards, the distance between the co-lead magnets was measured, each repeated three times to ensure reliable data collection. The measured distances were subsequently compared to the distances computed by the system and presented on the LCD interface. This systematic approach ensures precision in the experimental arrangement and directly compares the system's computations with the physically measured distances. The final step of this comparative analysis entails computing the Mean Squared Error (MSE), Mean Absolute Error (MAE), and Root Mean Squared Error (RMSE), which quantitatively evaluates the device's accuracy and how effectively it aligns with the calculated distances. This extensive testing procedure highlights the dedication to assessing the device's precision extensively and comprehensively.

D. CONTROL SCHEME USING HANDHELD DEVICE

1) CONTROL EXPERIMENT

Integrating the device with the inverter magnet represents significant advancement towards achieving accurate control over the catheter tip, thereby improving its maritime capabilities. The main objective of this experiment is to provide the catheter tip with 6 degrees of freedom (Figure 3a) by the precise medical requirements for successful lung intervention. The 6 degrees of freedom include movements in the X, Y, and Z axes for translation and roll, yaw, and pitch for rotation. Multi-dimensional control is essential for navigating the complex lung environment during medical procedures.

An adjustable model that acts as a comprehensive platform for testing and improving the control mechanism of the device. Due to its adaptable configurations, this model allows a broad spectrum of scenarios to assess the control system's efficiency and precision. The experiment aims to determine the most effective control strategy for achieving precise and responsive guidance of the catheter tip, utilising the adjustable model in various setups (Figure 3b). Additionally, the experiment seeks to validate the concept of manipulating the catheter tip through the device across multiple degrees of freedom. Two outlets were randomly selected for the navigation task. The first outlet has a length of 355.6mm, while the second is 345.44mm. The device guided the catheter tip towards each outlet five times. Outlet 1 presented a simple task for the user, as it involved following a direct path without any turns at bifurcations. On the other hand, accessing Outlet 2 required a more intricate manoeuvre; the user had to bend

the catheter tip to navigate a turn successfully. This additional step demonstrates the practical challenges encountered when manoeuvring a catheter through twists and turns in the body's blood vessels, assessing the device's capacity to navigate complex pathways.

The catheter is constructed from flexible, biocompatible materials, such as polydimethylsiloxane (PDMS), which ensure the device is both durable and safe for medical use. A neodymium-iron-boron (NdFeB) permanent magnet is embedded within the catheter, strategically positioned to interact optimally with the external magnetic field generated by the MTB system. The flexible nature of the PDMS material allows the catheter to navigate through confined and complex anatomical pathways with precision. These mechanical properties are essential for the effective steering and manoeuvrability of the catheter in minimally invasive procedures, ensuring it can be guided accurately by the magnetic field without causing damage to surrounding tissues.

The success rate, wall collisions, and time taken are recorded for each attempt. Subsequently, the average speed is calculated. The speed of catheter navigation was measured by calculating the distance travelled along the pathway and the time taken to traverse this distance. To quantify contact with the walls, we utilised an optical tracking system. This involved placing visual markers on the catheter and along the walls of the anatomical model. Cameras captured the catheter's movement and interactions with the walls in real-time. The recorded footage was then analysed to identify instances of contact and measure the duration and frequency of these interactions.

E. FABRICATION OF 3D PRINTED PHANTOM MODEL

Creating a 3D model of the trachea and bronchi through medical imaging involves using advanced imaging technologies such as MRI (Magnetic Resonance Imaging) and CT (Computed Tomography) scans. In the case of obtaining a detailed representation of the trachea and bronchi, a patient undergoes either an MRI or CT scan, both of which provide comprehensive views of internal anatomical structures. The obtained imaging data undergoes a series of steps, including image processing and segmentation, to isolate and distinguish the trachea and bronchi from surrounding tissues. Sophisticated software is employed to identify and extract the specific regions of interest, creating a set of 2D image slices. These slices are then reconstructed into a 3D model, preserving the intricate details of the trachea and bronchi. The choice between MRI and CT scans depends on factors such as resolution, contrast, and the clinical context, ensuring that the generated 3D model meets the specific requirements of the intended application.

The 3D realistic model (Figure 4), constructed from MRI and CT scans, was procured for experimentation. In the initial attempt, the model depicted in Figure 2a was 3D printed using an Ultimaker 3D printer and PLA materials. Following the initial fabrication, the process extended to creating a trachea and bronchi model with a 1:2 ratio size

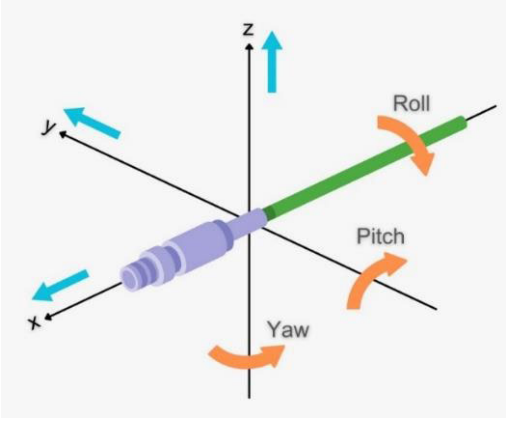

(a)

(b)

FIGURE 3. Experimental Setup for Control Scheme Evaluation a) Demonstration of the 6 degrees of freedom of the catheter tip. b) An example of the experimental configuration and procedure.

(Figure 4b). Recognising the practical constraints posed by its larger dimensions, the model was intelligently divided into four manageable parts. This strategic segmentation addressed the challenges associated with the size, rendering it more amenable to the printing process and subsequent assembly. The four segmented parts were then meticulously assembled using hot glue. Similarly, the realistic adult human-sized trachea and bronchi (Figure 4c) underwent the same procedure, being divided into four parts and printed using the Ultimaker. The subsequent steps involved assembling the segmented parts to create a comprehensive and anatomically accurate 3D representation. This method ensures the successful reproduction of intricate anatomical details while accommodating the limitations of the 3D printing process.

F. NAVIGATION EXPERIMENT WITH ULTRASOUND PROBE

Expanding on the practical design of the control scheme, the experimental focus now turns to utilising the 1:1 trachea and bronchi model, as previously introduced. Placed inside the water box, this anatomically precise model is crucial for

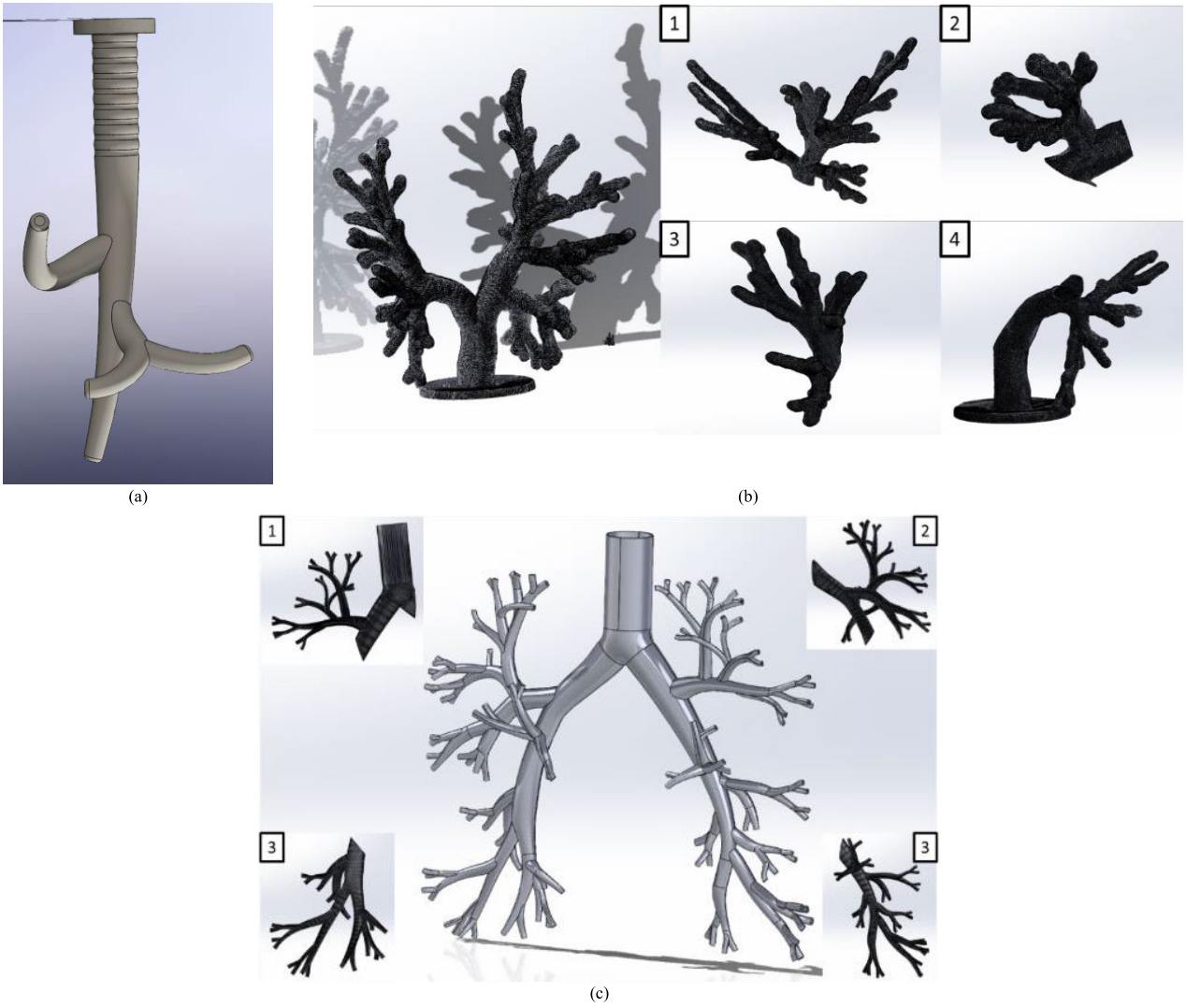

(a) (b) (c)

FIGURE 4. 3D Trachea and Bronchi model a) Trachea and primary bronchi model b) Small realistic trachea and bronchi model c) Realistic adult human size trachea and bronchi.

experimentation, as it creates a simulated environment that accurately mimics the complexities of navigating a catheter within the human body. The experiment incorporates an ultrasound probe, which provides real-time imaging capabilities. The ultrasound probe utilised in this setup is the MicrUs Pro-C60S, provided by the Telemed medical system. The accompanying software, Echo Wave II, enables users to view the real-time imaging outputs from the ultrasound probe. This allows users to continuously monitor the exact position of the catheter tip during the entire navigation procedure (Figure 5).

The catheter, which has a magnet at its tip, follows a precisely guided path using the handheld device. The catheter moves through the trachea and enters the bronchi, passing through various openings in the anatomical model. Multiple metrics are considered to assess the performance of the device thoroughly. The metrics encompass evaluating the efficacy of navigation, analysing occurrences of catheter tip-wall collisions, and quantifying navigation speed. The integration of these parameters yields a detailed comprehension of the device's functionality and efficacy in reproducing realistic navigation scenarios within the complex anatomical terrain of the respiratory system.

The experiment is conducted precisely, targeting each of the three outlets multiple times to generate a detailed dataset. Surgical planning software plays a crucial role in identifying tumours and determining the optimal path for the device (Figure 5c). This systematic approach ensures a comprehensive and representative analysis of the device's capabilities with outlets measuring 177.8mm, 406.4mm, and 325.12mm in length. The experiment is carried out ten times for each outlet, allowing for the calculation of the navigation success rate across all outlets, as well as the time required for each attempt. These metrics provide a holistic view of the device's navigational efficiency.

Considering all outlets, the catheter tip's average success rate and speed are computed to offer insights into the device's

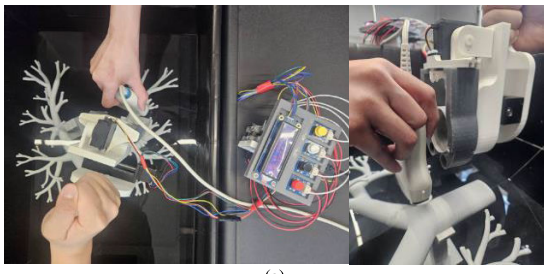

(a)

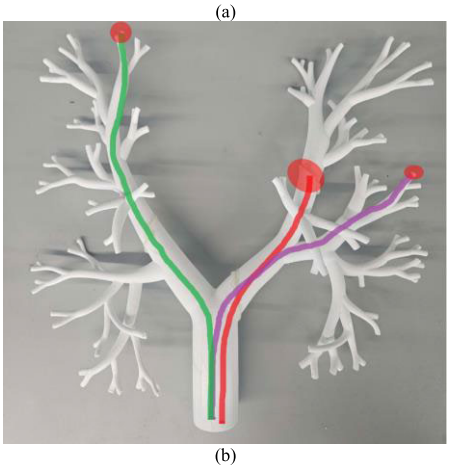

(b)

FIGURE 5. Navigation experiment setup a) Top view of the example of the experiment conducted using the handheld device and the ultrasound b) Side view of the example of the experiment conducted using the handheld device and the ultrasound c) 3 random tumours and the path identified by the surgical planning software. The red circle shows where the tumours are, while the colour line (green, red, purple) shows the path to the tumour.

performance in navigating complex pathways safely. The speed of catheter navigation is determined by measuring the pathway distance and the time required for the catheter to travel this distance. The navigation average speed is also calculated, presenting a quantitative assessment of the device's effectiveness in moving through the model's trachea and bronchi. This thorough examination aids in understanding the device's potential in real-world medical applications, emphasising its capacity to navigate intricate anatomical structures safely and efficiently.

III. RESULT AND DISCUSSION

A. MAGNETIC TRACTOR BEAM (MTB) DISTANCE

The reference table in Table 1 serves as a manual for regulating the follower magnet, which is integrated into the catheter tip. The table explicitly highlights the distances of co-lead magnets, which range from 9mm to 16mm, allowing for the MTB effect. The follower magnet has been noticeable for its versatility, varying from 6mm to as small as 1mm. A critical pattern can be identified from the data. As the size of the follower magnet increases, there is a proportional decrease in the distance between the lead and follower magnets, which is measured precisely from edge to edge. The complex relationship between the distance of co-lead magnets and the size of follower magnets highlights the dynamics of the magnetic tractor beam effect, giving users a clear understanding of the relationships that govern these critical parameters.

An analytical model was developed to predict the distance between lead and follower magnets using the distance between co-lead magnets and the diameter of the follower magnet. Linear regression models were constructed for each follower diameter after the data had been filtered and restructured. The results showed strong linear relationships with high R^2 values, indicating that the distance between lead and follower magnets can be accurately predicted based on the distance between co-lead magnets. A unified multiple linear regression model was created by combining individual models, yielding an equation with an R^2 value of around 0.958, indicating the model's strong ability to account for the data's variability. This model can predict the distance between the lead and follower magnets in millimetres using below:

$$\boldsymbol{Distance_{Lead-Follower}} = \mathbf{84.28} - \mathbf{3.21}\left(\boldsymbol{Distance_{Co-leads}}\right) - \mathbf{0.66}(\boldsymbol{Diameter_{Follower}})$$

The following predictions provided an accurate result for the scenario with a 12 mm distance between the co-lead and a 3 mm diameter follower, with only a 0.20% margin of error. A notable difference of around 9.31% was observed for the 15 mm gap between the leading and following components and a follower diameter of 5 mm. The model's MSE of 2.44, RMSE of 1.56, and MAE of 1.23 indicate its precision, with an average percentage error of 3.28%, confirming its overall effectiveness. The low error metrics highlight the model's precision, establishing it as a valuable predictive tool in magnetic bearing technology.

B. HANDHELD DEVICE

1) THE DEVICE

The assembly process is carried out using nylon screws to ensure the elimination of materials that can be attracted by magnets in the device. Every part, such as the gripper tip containing the co-lead magnets and the holder that keeps the lead magnet in place, is designed to form a uniform and effective device arrangement. The use of nylon screws improves the overall safety and efficacy of the device in the context of magnetic interactions. Users can easily adjust the distance between the co-lead magnets in this device configuration using buttons 1 and 2.

Button 3 enables the gripper to move, which allows the co-lead magnets to be positioned at a distance that prevents the Magnetic Tractor Beam (MTB) effect. In addition, activating button 4 causes the rail to move quickly in a straight line, going back and forth between the left and right sides simultaneously. The LCD screen offers immediate feedback by showing the ongoing movement of the device and presenting the current distance between the co-lead magnets. Table 2 offers a thorough overview of the control features of the device, serving as a convenient guide for users involved in experimental procedures. This variable control system

TABLE 1. Reference table for MTB magnets.

Distance between Co-lead magnets that enable MTB effects (mm)		Follower Magnet's Diameter					
		1	2	3	4	5	6
9	Distance between Lead and Follower magnets	54.33	53.67	53.67	53.67	53.67	51.67
10		54.33	50.67	50.67	50.33	49.33	49.33
11		49.33	46.67	46.33	46.00	45.00	44.67
12		45.67	44.67	43.67	43.33	42.00	41.67
13		41.33	39.00	38.67	38.33	38.00	37.67
14		37.33	37.00	36.67	36.33	36.33	35.67
15		36.67	36.67	36.33	36.00	35.00	34.67
16		36.51	36.11	35.41	35.11	34.51	34.21

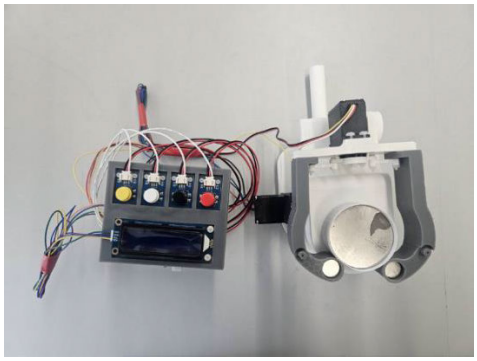

FIGURE 6. The Handheld device.

was designed to ensure optimal and accurate manipulation, enhancing user-friendliness during operation.

TABLE 2. Reference guide for the device control features.

Button 1 (White button)	Co-lead magnet moves closer by 1mm
Button 2 (Yellow button)	Co-lead magnet moves further by 1mm
Button 3 (Black button)	Linear motion of Inverter magnet - 50mm translation
Button 4 (Red button)	Move the co-lead magnet further away so the MTB effect doesn't occur

2) DISTANCE BETWEEN CO-LEAD MAGNET AND THE ACCURACY

The construction of the reference table has been executed using SolidWorks assembly, capturing the servo motor angles with the initial position set at 0° and their corresponding conversion into the distances between co-lead magnets. This detailed analysis reveals that, at the servo motor's initial position, the distance between co-leads measures 31.81mm. Conversely, when the distance between co-leads reaches its minimum of 8.8mm, the servo motor is positioned at 76.19 °. This establishes a valuable ratio, indicating that a 3.3113° servo motor turn corresponds to a 1mm change in the distance between co-leads. This leads to the equation below:

$$Servo_{position} = 3.113(31.81 - Co - leads_{distance})$$

where the $Servo_{position}$ is in degree and $Co - leads_{distance}$ is in millimetres. After assembling the 3D-printed handheld device, the distance between the co-lead magnets is meticulously measured and compared with the system-reported distance. This comparative analysis yields several key error metrics: Mean Squared Error (MSE) stands at 0.2, Mean Absolute Error (MAE) is 0.30, and Root Mean Squared Error (RMSE) is calculated to be 0.4. These metrics indicate the measurements' precision and accuracy, with lower values signifying a closer match between the "System Distance" and the "Actual Distance." Furthermore, the Mean Percentage Error (MPE) is approximately -1%. The negative sign in the MPE suggests that, on average, the system-reported distances are marginally less than the actual measured distances by about 1 %, highlighting a slight systematic underestimation in the system's distance measurements.

C. CONTROL SCHEME OF THE DEVICE

1) CONTROL SCHEME

The mechanism employs MTB effects to precisely control a device through multiple planes and angles. Precisely, the y-plane corresponds to the y-plane (left and right), and the z-plane represents vertical movements (up and down), as well as controlling yaw (rotation around the vertical axis) and pitch (tilt forward or backwards), the system utilises the interaction between co-lead magnets and an inverter magnet. By adjusting the proximity of the co-lead magnets—bringing them closer or moving them further apart—the user can finely regulate the distance between the inverter magnet primarily in the z-plane. This regulation is crucial for manoeuvring the inverter magnet, which, in turn, guides the follower magnet. The follower magnet is designed to maintain a constant gap from the inverter magnet, mirroring its movements. Through this magnetic coupling, the inverter magnet can effectively command the follower magnet to navigate through the y and z planes. Additionally, it enables the execution of yaw and pitch

motions, allowing for a comprehensive range of movements essential for navigating complex pathways.

MTB effects for this objective is an advanced method that uses magnetic fields to manipulate objects without physical contact, providing excellent precision and responsiveness. This approach not only simplifies the control mechanism but also improves the safety and efficiency of the navigation process by reducing the physical resistance commonly encountered with mechanical linkages. As a result, users can attain a smooth and intuitive control experience, which is essential for tasks that demand careful manipulation and accurate motions, such as medical procedures.

The user manipulates the inverter magnet by utilising the linear motion mechanism integrated into the handheld device, specifically along the x-axis, representing the forward and backward direction in spatial terms. This mechanism enables efficient manipulation of the inverter magnet, essential to controlling the follower magnet and the catheter tip along the x-plane. Figure 7a shows the planned path and motion of the inverter magnet. Based on Figure 7b, the positioning of the inverter magnet requires precise alignment of the magnets. Notably, the inverter magnet must be positioned so that only one-half of it aligns with one-half of the follower magnet. Precise alignment is crucial for the effective interaction of magnetic forces, allowing for controlled movement of the follower magnet.

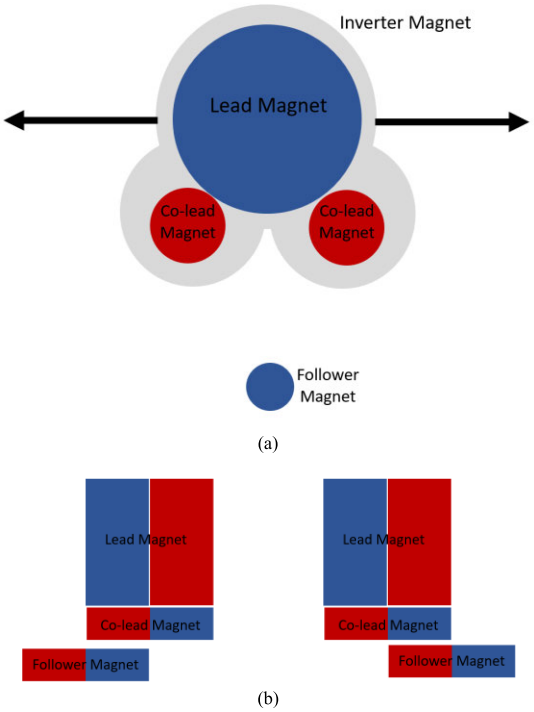

FIGURE 7. Example of the control scheme where the inverter is used to manipulate the catheter tip in x-plane (forward and backwards).

The handheld device has a linear rail that lets the user move the inverter magnet 25mm to the left and right. This movement can be achieved at a speed of 55 rpm. The controlled movement enables the tail of the follower magnet to rotate approximately 10 degrees towards the direction in which the inverter magnet has been displaced. The user can make minor lateral adjustments by manipulating magnetic forces, precisely the attraction and repulsion between the lead and co-lead magnets. These fine movements allow the user to guide the follower magnet with high precision, critical when the magnet is in a restricted or delicate area, such as the airway in medical settings. However, the user must manually adjust roll motion, which involves rotating the catheter along its longitudinal axis. These modifications ensure the catheter tip can be accurately aligned with the movements caused by the magnet. Table 3 summarises the methods used by the handheld device to control the catheter tip. It includes details regarding the user interactions needed for each type of movement, including the manual roll motion.

TABLE 3. Reference guide for the catheter tip control.

Degree of Freedom	Motion
X-plane	Linear motion of inverter magnet
Y-plane	MTB effects
Z-plane	MTB effects
Yaw	MTB effects
Pitch	MTB effects
Roll	Manually

2) PRELIMINARY CONTROL EXPERIMENT

Once a control scheme for the device had been developed, a set of trials was carried out using the handheld device to manipulate the catheter tip. The catheter tip is attached to different size follower magnets and moved within a model that can be adjusted. The utilised follower magnets varied in diameter from 1mm to 3mm. The experimental data highlights critical exploration. When the operator can visually perceive the location of the catheter tip, the success rate of navigating the catheter reaches 100%, with an average movement speed of 13.78mm/s and an average occurrence of 5 wall collisions.

The data (Figure 8a) also indicates a significant difference in the performance between the two tested outlets. Outlet 1 exhibited more incredible speed and a shorter duration for the catheter tip to reach the target point than Outlet 2. The complex structure of the model can explain the difference. Outlet 1 provides a direct route without any turns, while Outlet 2 has a bifurcation that requires bending and precise control of the catheter tip in a specific direction. The need for enhanced directional control in Outlet 2 necessarily results in more collisions with walls, as the user is required to navigate the catheter tip around bends in the pathway.

Furthermore, the graphs in Figure 8b show a clear and direct relationship between the size of the follower magnet and the rate of collisions with the wall. A greater diameter of the follower magnet correlates with a higher rate of collisions with the wall in Outlet 2. This is because the navigation in

Outlet 2 is more complicated, as it requires the catheter to bend. Conversely, the rate of collisions in Outlet 1 remains constant regardless of the size of the magnet since the direct path does not require any turn. The average rate of collisions with walls for Outlet 1 is 1, indicating a smoother navigation experience. However, for Outlet 2, this rate increases to 9, indicating the difficulties presented by navigating turns.

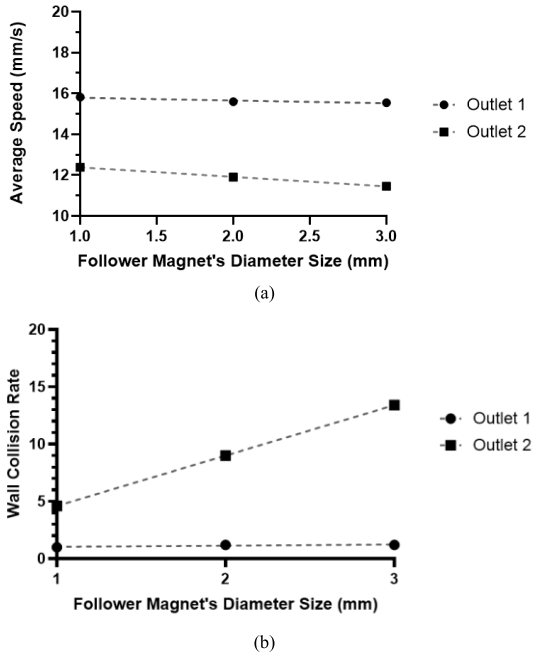

FIGURE 8. The control scheme experiment where different follower magnet diameter size shows different speed and wall collision rates. (a) Average speed in each follower magnet's diameter size (b) Wall collision rate in each follower magnet's diameter size.

These findings indicate that the visibility of the catheter tip influences the catheter's success rate, the pathway's complexity and the follower magnet's size. These factors significantly affect the efficiency and accuracy of the catheter's navigation. These findings are essential for enhancing the design and control of catheter-guidance systems, especially in medical applications where the capability to navigate complex structures is the highest priority. The data demonstrates the capabilities of the control scheme and handheld device and guides future enhancements in similar systems.

D. EXPERIMENT MODEL

1) SIMPLE TRACHEA AND PRIMARY BRONCHI MODEL

The initial stage of this process involves utilising the capabilities of the Ultimaker 3D printer to create an accurate Trachea and Bronchi model proportional to its real-life size (Figure 9). This process utilises white PLA material with a 100% infill, ensuring the structure's strength and accuracy. The model's dimensions are well-suited to the capacity of the 3D printer, eliminating the requirement to divide it into smaller parts before printing. The anatomical replica is produced with a minimum diameter of 6mm, a maximum diameter of 25mm, and a thickness of 4mm. The stand is precisely cut using laser technology to enhance stability, ensuring a secure base and a horizontal point of attachment for the model during experimentation. In addition, to improve the visual clarity of the experimental setup, different coloured tapes are strategically attached to the outlet of the model. This helps to identify and distinguish the various components quickly. This manufacturing process guarantees that the Trachea and Bronchi model meets rigorous precision standards and provides practical usefulness for comprehensive experimentation.

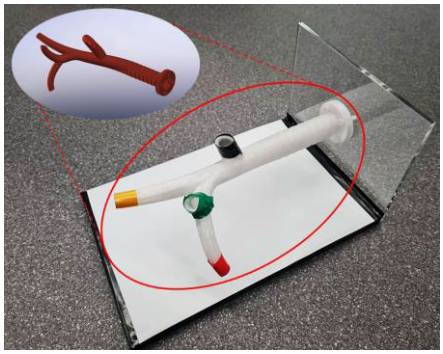

FIGURE 9. Trachea and bronchi of the 3D printed model with a stand and Model in Solidworks.

2) TRACHEA AND BRONCHI MODEL

The utilisation of the segmented printing strategy in Ultimaker ensures practicality and highlights the versatility of the resulting trachea and bronchi models. The intentional decision to provide an adhered 1:1 version, as shown in Figure 10, brings about a benefit. When operating independently, each segment functions as a separate module for conducting more straightforward experiments, enabling researchers to investigate specific model elements before engaging in a more complex setup.

FIGURE 10. Realistic 3D printed adult Trachea and bronchi model.

This method provides a clear route, beginning with separate sections linked to a water container for regulated experiments. The design's modularity enables researchers to

precisely adjust variables and gain a comprehensive understanding of the model's behaviour in isolation. As experiments progress, the possibility of creating a 1:1 trachea and bronchi model that fits together perfectly becomes more and more likely. When connected to a water box, this complete model is a foundation for conducting more complex experiments, allowing for a smooth progression from simpler setups to advanced investigations. The flexibility of this printing and assembly method optimises the model's usefulness, accommodating a range of experimental requirements and enhancing the analysis of tracheal and bronchial dynamics.

E. NAVIGATION EXPERIMENT WITH ULTRASOUND PROBE

The navigation experiment, aimed at simulating a realistic environment, utilised the Trachea and Bronchi Model, navigating the catheter tip attached to a follower magnet through the model with a handheld device. The entire model was submerged in a water-filled box to mimic the conditions encountered during medical procedures. An ultrasound probe was deployed, allowing the operator to track the catheter tip in real time, effectively replicating the visibility constraints and tracking challenges faced during bronchoscopy procedures (Figure 11a). During the experiment, the minor outlet in the model measured 1.2mm in diameter, necessitating a follower magnet with a 1mm diameter. The lack of transparency in the model meant that the operator could not visually locate the catheter tip and had to rely solely on ultrasound imaging for navigation. The success rate in this scenario was 80%, illustrating the difficulty of guiding the catheter tip without direct visual cues. The occasional collisions with the model's walls, leading to the catheter tip becoming stuck, underscore the need for enhanced ultrasound visualisation to continue precise control over the catheter movement.

Furthermore, the average speed of catheter navigation was recorded at 5.2mm/s. When comparing the bifurcations along each coloured path—red, green, and purple—representing the three outlets, it was found that the red path, with only one bifurcation, allowed for the fastest catheter travel. The green path with two bifurcations was slightly slower, and the purple path with three was the slowest (Figure 11b). This correlation suggests that the number of bifurcations directly affects the average speed and time to navigate each path. Additionally, the number of bifurcations had a measurable impact on the success rate. With its singular bifurcation and broader diameter, the red path facilitated a 100% success rate, indicating that larger pathway diameters improve the ease with which the catheter can be guided to the target (Figure 11c). This finding aligns with data from previous control experiments, which indicated that pathway diameter plays a crucial role in the success rate and the likelihood of wall collisions.

An analysis of the current experiment about previous experiments demonstrates the significant impact that visual tools, such as ultrasound, have on the effectiveness of navigation. When visibility is limited, even the most advanced control systems can encounter decreased effectiveness,

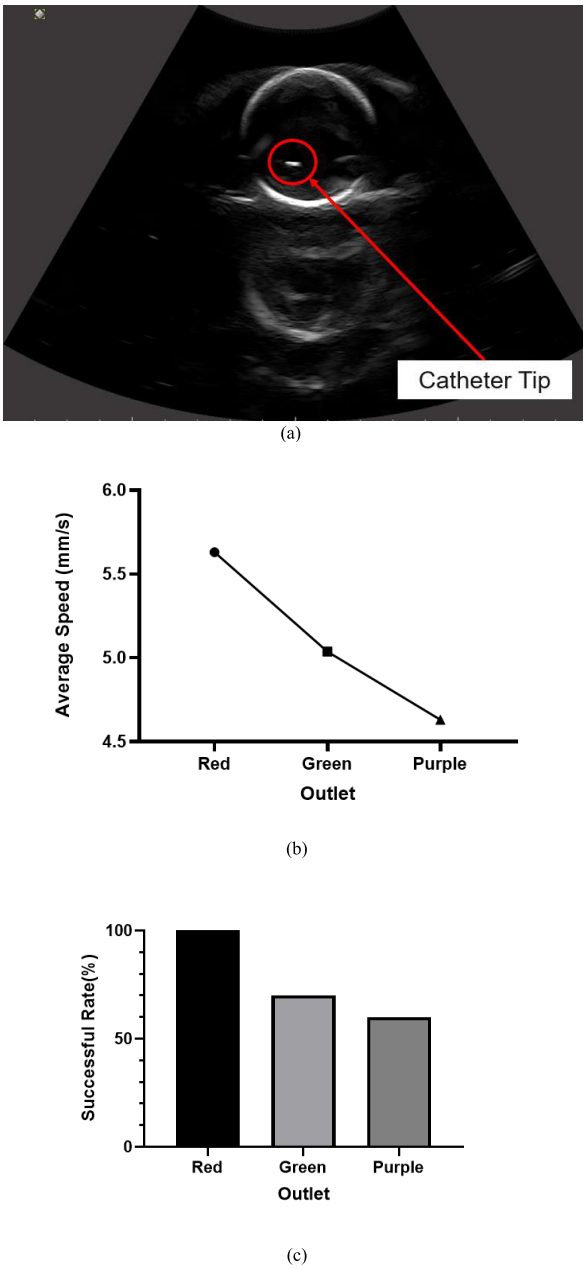

FIGURE 11. The experiment result of the navigation experiment a) Example of the user was able to see the catheter tip through the ultrasound probe b) Average speed in each outlet c) Wall collision rate in each outlet.

highlighting the significance of clear visualisation combined with accurate device control. The data indicates a requirement for improvements in real-time imaging methods to enhance the precision and dependability of catheter navigation, ultimately leading to better patient outcomes in procedures that depend on this technology.

IV. CONCLUSION

The study's thorough study and development have resulted in significant insights and technological advancements in medical device engineering. The intended goals in developing and

constructing a magnetic tractor beam (MTB) device and the precise techniques implemented have significantly improved control and guided catheter-based interventions. The systematic approach to choosing the most suitable magnet dimensions has been crucial in maximising the strength of the magnetic field and improving the MTB effect. Enhancements of such features are crucial in ensuring the manoeuvrability of the follower magnet within the narrow and complex bronchial pathways, a significant challenge in the field of pulmonary interventions.

Integrating a handheld device designed to manipulate the magnetic interactions required for guiding a catheter signifies a significant advancement in versatility and user control. Integrating mechanical design, electronic components, and cautious material selection has resulted in a robust and user-friendly device capable of performing complex navigational tasks. During the experiments, the device consistently demonstrated a high success rate, robust control over multiple degrees of movement, and the possibility of being used in real-life lung interventions. The significant difference in performance among various pathways has highlighted the importance of using real-time visual tracking methods, such as ultrasound, to position the catheter tip precisely. The accurate positioning of the catheter tip directly impacts the procedure's success.

The control mechanisms of the MTB handheld device are designed to enhance user interaction through intuitive and precise controls. The device features four buttons and an LCD screen to facilitate user input and provide real-time feedback. The servo motor, responsible for adjusting the distance between the co-lead magnets, and the stepper motor, controlling linear movement along the rail, are easily managed via these buttons, allowing smooth and accurate adjustments. The LCD screen displays information, such as the distance between the co-lead magnets, giving users immediate and continuous feedback during operation.

Specific user feedback metrics gathered during the experimental validation process included the success rate of catheter navigation, the number of wall collisions, and the time taken to reach target points within the anatomical model. Users reported high levels of satisfaction with the device's responsiveness and the clarity of the real-time feedback. The metrics indicated a higher navigation success rate, fewer collisions, and faster navigation times compared to traditional methods, demonstrating that the control mechanisms significantly improve the accuracy of catheter manipulation and the overall user experience.

The results underline the critical significance of visibility, pathway diameter, and precise control when navigating complicated anatomical structures. To move from controlled experimental settings to real medical scenarios, the understanding obtained from this research offers an optimistic perspective for the future of minimally invasive procedures. There is a need for ongoing development of imaging techniques to give medical professionals the most effective tools for performing vital surgeries.

Ultimately, this research has not only filled an oversight in the understanding of magnetic control systems but also created an improved assessment of the accuracy of medical devices. The MTB device demonstrates the innovation and capacity of engineering to enhance patient care and advance the progress of medical technology. It envisions a future where healthcare professionals widely use these tools, guiding patient treatment towards safer and more effective outcomes.

REFERENCES

[1] A. P. Advincula and K. Wang, "Evolving role and current state of robotics in minimally invasive gynecologic surgery," *J. Minimally Invasive Gynecol.*, vol. 16, no. 3, pp. 291–301, May 2009.

[2] C. Chautems, A. Tonazzini, Q. Boehler, S. H. Jeong, D. Floreano, and B. J. Nelson, "Magnetic continuum device with variable stiffness for minimally invasive surgery," *Adv. Intell. Syst.*, vol. 2, no. 6, Jun. 2020, Art. no. 1900086.

[3] Y. Fu, H. Liu, W. Huang, S. Wang, and Z. Liang, "Steerable catheters in minimally invasive vascular surgery," *Int. J. Med. Robot. Comput. Assist. Surg.*, vol. 5, no. 4, pp. 381–391, Dec. 2009.

[4] M. R. Hsu, M. S. Haleem, and W. Hsu, "3D printing applications in minimally invasive spine surgery," *Minimally Invasive Surg.*, vol. 2018, pp. 1–8, Apr. 2018.

[5] X. Hu, A. Chen, Y. Luo, C. Zhang, and E. Zhang, "Steerable catheters for minimally invasive surgery: A review and future directions," *Comput. Assist. Surg.*, vol. 23, no. 1, pp. 21–41, Jan. 2018.

[6] H. N. Kim, X. N. Liu, and K. C. Noh, "Use of a real-size 3D-printed model as a preoperative and intraoperative tool for minimally invasive plating of comminuted midshaft clavicle fractures," *J. Orthopaedic Surg. Res.*, vol. 10, no. 1, pp. 1–6, Dec. 2015.

[7] C. Limpabandhu, Y. Hu, H. Ren, W. Song, and Z. T. H. Tse, "Actuation technologies for magnetically guided catheters," *Minimally Invasive Therapy Allied Technol.*, vol. 32, no. 4, pp. 137–152, Aug. 2023.

[8] J. H. Palep, "Robotic assisted minimally invasive surgery," *J. Minimal Access Surg.*, vol. 5, no. 1, pp. 1–7, 2009.

[9] H. Su, A. Mariani, S. E. Ovur, A. Menciassi, G. Ferrigno, and E. De Momi, "Toward teaching by demonstration for robot-assisted minimally invasive surgery," *IEEE Trans. Autom. Sci. Eng.*, vol. 18, no. 2, pp. 484–494, Apr. 2021.

[10] H. Chung, A. M. Parsons, and L. Zheng, "Magnetically controlled soft robotics utilizing elastomers and gels in actuation: A review," *Adv. Intell. Syst.*, vol. 3, no. 3, Mar. 2021, Art. no. 2000186.

[11] N. Ebrahimi, C. Bi, D. J. Cappelleri, G. Ciuti, A. T. Conn, D. Faivre, N. Habibi, A. Hošovský, V. Iacovacci, I. S. M. Khalil, V. Magdanz, S. Misra, C. Pawashe, R. Rashidifar, P. E. D. Soto-Rodriguez, Z. Fekete, and A. Jafari, "Magnetic actuation methods in bio/soft robotics," *Adv. Funct. Mater.*, vol. 31, no. 11, Dec. 2020, Art. no. 2005137.

[12] C. M. Heunis, Y. P. Wotte, J. Sikorski, G. P. Furtado, and S. Misra, "The ARMM system–autonomous steering of magnetically-actuated catheters: Towards endovascular applications," *IEEE Robot. Autom. Lett.*, vol. 5, no. 2, pp. 705–712, Apr. 2020.

[13] S. Jeon, G. Jang, H. Choi, and S. Park, "Magnetic navigation system with gradient and uniform saddle coils for the wireless manipulation of micro-robots in human blood vessels," *IEEE Trans. Magn.*, vol. 46, no. 6, pp. 1943–1946, Jun. 2010.

[14] S. W. Hetts, M. Saeed, A. J. Martin, L. Evans, A. F. Bernhardt, V. Malba, F. Settecase, L. Do, E. J. Yee, A. Losey, R. Sincic, P. Lillaney, S. Roy, R. L. Arenson, and M. W. Wilson, "Endovascular catheter for magnetic navigation under MR imaging guidance: Evaluation of safety *in vivo* at 1.5T," *Amer. J. Neuroradiol.*, vol. 34, no. 11, pp. 2083–2091, Nov. 2013.

[15] S. M. Jeon and G. H. Jang, "Precise steering and unclogging motions of a catheter with a rotary magnetic drill tip actuated by a magnetic navigation system," *IEEE Trans. Magn.*, vol. 48, no. 11, pp. 4062–4065, Nov. 2012.

[16] L. Müller, M. Saeed, M. W. Wilson, and S. W. Hetts, "Remote control catheter navigation: Options for guidance under MRI," *J. Cardiovascular Magn. Reson.*, vol. 14, no. 1, pp. 1–9, Jan. 2012.

[17] Z. Yang, L. Yang, M. Zhang, C. Zhang, S. C. H. Yu, and L. Zhang, "Ultrasound-guided catheterization using a driller-tipped guidewire with combined magnetic navigation and drilling motion," *IEEE/ASME Trans. Mechatronics*, vol. 27, no. 5, pp. 2829–2840, Oct. 2022, doi: 10.1109/TMECH.2021.3121267.

[18] M. P. Armacost, J. Adair, T. Munger, R. R. Viswanathan, F. M. Creighton, D. T. Curd, and R. Sehra, "Accurate and reproducible target navigation with the Stereotaxis Niobe magnetic navigation system," *J. Cardiovascular Electrophysiol.*, vol. 18, no. s1, pp. S26–S31, Jan. 2007.

[19] F. Carpi and C. Pappone, "Stereotaxis Niobe magnetic navigation system for endocardial catheter ablation and gastrointestinal capsule endoscopy," *Expert Rev. Med. Devices*, vol. 6, no. 5, pp. 487–498, Sep. 2009.

[20] A. W. Mahoney and J. J. Abbott, "Generating rotating magnetic fields with a single permanent magnet for propulsion of untethered magnetic devices in a lumen," *IEEE Trans. Robot.*, vol. 30, no. 2, pp. 411–420, Apr. 2014.

[21] S. Tognarelli, V. Castelli, G. Ciuti, C. Di Natali, E. Sinibaldi, P. Dario, and A. Menciassi, "Magnetic propulsion and ultrasound tracking of endovascular devices," *J. Robotic Surg.*, vol. 6, no. 1, pp. 5–12, Mar. 2012.

[22] J. Hwang, J.-Y. Kim, and H. Choi, "A review of magnetic actuation systems and magnetically actuated guidewire- and catheter-based microrobots for vascular interventions," *Intell. Service Robot.*, vol. 13, no. 1, pp. 1–14, Jan. 2020.

[23] C. Limpabandhu, Y. Hu, H. Ren, W. Song, and Z. Tse, "Towards catheter steering using magnetic tractor beam coupling," *Proc. Inst. Mech. Eng., H, J. Eng. Med.*, vol. 236, no. 4, pp. 583–591, Apr. 2022.

CHAYABHAN LIMPABANDHU received the Bachelor of Engineering degree in electronics and communication engineering from the Sirindhorn International Institute of Technology, Thammasat University, and the Master of Science degree in intelligence systems and robotics from the University of Essex. She is currently pursuing the Ph.D. degree in medical engineering with the Queen Mary University of London's Digital Health and Robotics Laboratory, focusing on magnetically actuated devices for medical interventions. Her academic journey and professional experiences are deeply rooted in the advancement of medical device technology, particularly in the integration of robotics and magnetic actuation in healthcare applications. Her contributions to interdisciplinary projects and academic competitions highlight her dedication to innovation in the fields of digital health and medical engineering.

ZION TSZ HO TSE received the Ph.D. degree in mechatronics in medicine from Imperial College London, U.K. He is currently an Academy of Medical Sciences Professor of digital health and robotics and the Director of the Centre for Bioengineering, Queen Mary University of London. Prior to that, he was the Chair Professor of the University of York, and an Associate Professor with the University of Georgia. Before that, he was a Research Fellow with Harvard University, Boston, Massachusetts. Most of his academic and professional experience has been in AI, digital health, medical robotics, and imaging. He has been developing and testing a broad range of medical technologies in his career, most of which have been applied in clinical patient trials. His research bridges engineering and medicine, connecting multidisciplinary teams of medical doctors, researchers, and engineers.